Chiral Chemistry

Science Exploration

Open Access Research Article

Enantiopure chiral multilayer polymers – design, asymmetric synthesis and property study

Hao Liu[1], Qingkai Yuan[1], Delgado Cordoba Lina[1], Zacheaus M. Akinpelu[1], My Phan[1], Hongjun Liang[2], Anthony F. Cozzolino[1], Dimitri Pappas[1], Guigen Li[1,*]

[1]Department of Chemistry and Biochemistry, Texas Tech University, Lubbock, TX 79409, USA.
[2]Department of Cell Physiology Molecular Biophysics, School of Medicine, Texas Tech University Health Sciences Center, Lubbock, TX 79430, USA.

***Correspondence to:** Guigen Li, Department of Chemistry and Biochemistry, Texas Tech University, Lubbock, TX 79409, USA. E-mail: guigen.li@ttu.edu

Received: February 13, 2026 **Accepted:** April 08, 2026 **Published:** April 08, 2026

Cite this article: Liu H, Yuan Q, Lina DC, Akinpelu ZM, Phan M, Liang H, et al. Enantiopure chiral multilayer polymers – design, asymmetric synthesis and property study. Chiral Chem. 2026;2:202609. https://doi.org/10.70401/cc.2026.0020

Abstract

Axially chiral binaphthyl scaffolds provide a robust platform for encoding permanent stereochemistry into conjugated polymer backbones while promoting nonplanar organization and higher-order aggregation. Building on our group's earlier development of multilayer 3D folding polymers and related achiral/chiral multilayer polymer series, we designed and synthesized the first enantiopure chiral multilayer polymers from enantiopure binaphthyl-derived monomers via CuI-assisted, Pd-catalyzed Sonogashira polycondensation. To probe structure–property relationships, the monomer library was designed to contrast flexible alkoxy-substituted systems with a conformationally constrained tethered analogue. The resulting polymers were obtained in moderate yields, with number-average molecular weights on the order of 10^3-10^4 g mol^{-1} and relatively narrow dispersities. UV–visible spectra showed the expected aromatic π-π* absorptions. Photoluminescence measurements in tetrahydrofuran (THF)/H_2O mixtures displayed a nonmonotonic solvent-composition dependence, with emission enhancement at intermediate water fractions followed by quenching in more water-rich mixtures. Dynamic light scattering indicated the presence of light-scattering dispersed aggregates in $CHCl_3$ under the tested conditions, while scanning electron microscopy revealed hierarchical agglomerates in the dried state, in which submicrometer particulates coalesced into micrometer-scale clusters. Together, these results show that axial stereochemistry and aggregation/packing behavior cooperatively influence radiative and nonradiative decay pathways in chiral multilayer backbones, providing useful design guidance for aggregation-responsive emissive polymer materials.

Keywords: Axial chirality, chiral multilayer polymers, 3D folding polymers, circular dichroism, aggregation-induced emission, aggregation-responsive photophysics

1. Introduction

1.1 Axial chirality in polymer backbones: motivation and prior art

Encoding permanent stereochemical information into the main chain of conjugated polymers remains an important objective in the design of chiral functional materials. Among the available chiral motifs, 1,1'-binaphthyl (BINOL/BINAP-type) scaffolds are particularly attractive because of their robust atropisomerism and intrinsically twisted geometry[1]. In contrast to point chirality, which is often introduced through pendant, and conformationally flexible substituents, the rigid binaphthyl axis can be incorporated directly into the polymer backbone. This structural feature makes it possible to translate monomer-level chirality into macromolecular conformational bias and higher-order organization, thereby strongly influencing chiroptical responses and packing behavior[2]. Early studies showed that binaphthyl-containing polymer backbones can amplify chiral expression and bias chain conformation. At the same time, their contorted and shape-persistent structures often remain compatible with solution processing, making them attractive platforms for optically active materials with distinctive stacking preferences and porous or aggregation-prone architectures.

1.2 From multilayer 3D folding architectures to enantiopure chiral multilayer polymers

Multilayer 3D architectures introduce an additional structural level for expressing chirality, because constrained interlayer packing and restricted rotation between aromatic components can generate cooperative stereochemical outputs. Building on our group's

© The Author(s) 2026. This is an Open Access article licensed under a Creative Commons Attribution 4.0 International License (https://creativecommons.org/licenses/by/4.0/), which permits unrestricted use, sharing, adaptation, distribution and reproduction in any medium or format, for any purpose, even commercially, as long as you give appropriate credit to the original author(s) and the source, provide a link to the Creative Commons license, and indicate if changes were made.

earlier asymmetric catalytic assembly of multilayer 3D chiral folding polymers[3] and the subsequent development of achiral/chiral multilayer polymer series[4], we sought to extend this platform to *enantiopure* chiral multilayer polymers. In the present context, the term "enantiopure" emphasizes that the macromolecular chirality is derived directly from enantiopure monomer feedstocks. This design provides structurally matched *R*- and *S*-polymer pairs, enabling a more direct evaluation of stereochemical fidelity, and offering well-defined model systems for examining how axial chirality, backbone geometry, and aggregation behavior become coupled in multilayer polymer frameworks.

1.3 Design strategy and scope of this work

In this study, we use axial chirality as the primary design element to construct main-chain polymers from a family of enantiopure 8,8'-dibrominated binaphthyl monomers based on a common 7,7'-dimethoxy scaffold. Within this framework, the steric and electronic environment around the chiral axis is systematically modulated: the 2,2'-positions are functionalized either with a series of alkoxy substituents of different steric demand or with a conformationally constraining dioxine bridge[5,6]. The 8,8'-dibromo groups serve as cross-coupling handles for Sonogashira polycondensation, thereby embedding the binaphthyl twist into the conjugated backbone. Meanwhile, variation at the 2,2'-positions modulates local steric congestion without changing the core connectivity. We anticipated that these structural changes would influence accessible dihedral angles, interchain packing within the multilayer arrangement, and solvent-dependent aggregation behavior[7].

In addition, the choice of bridge linker is an important part of the present molecular design. We selected *1,8*-diethynylnaphthalene as the diyne bridge because its sterically congested *1,8*-substitution pattern is more compatible with the targeted nonplanar multilayer backbone. By contrast, more extended and relatively linear diyne linkers, such as *1,4*-diethynylnaphthalene or *1,4*-diethynylbenzene, would be expected to promote different backbone geometries, packing modes, and aggregation behavior. A systematic comparison of linker effects is therefore of clear interest, but it lies beyond the scope of the present study.

Beyond structural design, the aggregation behavior of axially chiral aromatic polymers is of particular interest because packing mode can strongly influence excited-state dynamics. In aromatic systems, emission outcomes are often closely tied to aggregation state: restriction of intramolecular motion can enhance emission[8,9], whereas overly dense π-stacking may lead to emission quenching[10]. Accordingly, we treat photophysical and morphological characterizations not simply as performance descriptors, but also as probes for understanding how monomer-level stereochemistry and backbone sterics shape assembly across multiple length scales.

Enantiomeric polymer pairs (**1A**–**3A**) were prepared to evaluate stereochemical fidelity and chiroptical expression, while the broader monomer set, incorporating both linear and cyclic substituents, enables discussion of how substituent environments affect polymerization outcome, aggregation tendency, and solid-state organization. By combining circular dichroism (CD) with complementary spectroscopic and morphological analyses, we aim to establish a structure–property framework for binaphthyl-derived chiral multilayer polymers and to clarify how axial stereochemistry, backbone geometry, and aggregation behavior collectively govern their optical response.

2. Experimental

2.1 Materials and general procedures

Unless otherwise noted, commercially available reagents were used as received. Moisture- and air-sensitive reactions were carried out under an inert atmosphere using oven-dried glassware. Solvents were purified and/or dried following standard laboratory practice, when necessary. Detailed experimental procedures, purification protocols, and full characterization datasets are provided in the Supplementary Materials.

2.2 Preparation of axially chiral monomers

Synthesis of the axially chiral 8,8'-dibrominated binaphthyl monomers was achieved by adapting reported procedures[11,12]. Comprehensive experimental details, including purification steps and spectroscopic data for all intermediates, are provided in the Supplementary Materials. Enantiomeric enrichment was verified via chiral high-performance liquid chromatography (HPLC). In the specific case of the bridged monomer (**6S**), where baseline separation was not attainable on standard chiral stationary phases, stereochemical integrity was supported by specific optical rotation analysis (Supplementary Materials).

2.3 General procedure for Sonogashira polycondensation

Polymers were synthesized via CuI-assisted, Pd-catalyzed Sonogashira polycondensation in toluene/triethylamine under an inert atmosphere. A representative procedure, including catalyst loading, monomer stoichiometry, concentration, temperature, and workup protocol, is provided in the Supplementary Materials for reproducibility. Polymer yields were calculated as isolated yields after purification.

2.4 Instrumentation and characterization

2.4.1 Nuclear magnetic resonance (NMR)

^{1}H and ^{13}C NMR spectra were recorded on a JEOL ECS 400 MHz spectrometer. Chemical shifts (δ) are reported in parts per million (ppm) relative to tetramethylsilane (TMS). Residual solvent resonances served as internal references; full spectral datasets are provided in the Supplementary Materials.

2.4.2 Optical rotation

Specific optical rotations ($[\alpha]_D$) were determined at ambient temperature using a Rudolph Research Analytical AUTOPOL IV automatic polarimeter (model APIV/2W). Analysis was performed in spectroscopic-grade chloroform ($CHCl_3$) at a concentration of c = 0.5 mg mL^{-1}.

2.4.3 UV–visible spectroscopy (UV)

UV–vis absorption spectra were recorded on an Agilent 8,453 diode-array UV–visible spectrophotometer (wavelength range 190–1,100 nm; nominal spectral slit width 1 nm; mean sampling interval ~0.9 nm). Polymer solutions were prepared in $CHCl_3$ (c = 0.05 mg mL^{-1}) and measured in quartz cuvettes with a 1 cm optical path length, using a $CHCl_3$ blank for baseline subtraction. Unless otherwise noted, spectra shown in the main text are discussed over 190–800 nm.

2.4.4 Gel permeation chromatography (GPC)

Molecular weight distributions were determined using a TOSOH Eco SEC HLC-8320 system equipped with a dual-flow refractive index (RI) detector. The mobile phase was THF delivered at a flow rate of 1.0 mL min^{-1} (40 °C). To prevent column blockage and ensure homogeneous injection under the higher-concentration gel permeation chromatography (GPC) conditions, polymer samples were dissolved in THF containing 10 vol% $CHCl_3$, filtered through a 0.22 μm PTFE syringe filter, and injected (10 μL). Calibration was based on polystyrene (PS) standards (PStQuick C) covering 500–10^7 Da.

2.4.5 Circular dichroism (CD)

CD spectra were recorded on a JASCO J-815 spectropolarimeter equipped with a photomultiplier tube (PMT) detector (voltage mode: auto). Measurements were performed in continuous-scan mode over a wavelength range of 400–245 nm with a scanning speed of 100 nm min^{-1} a spectral bandwidth of 1.0 nm, a data pitch of 0.1 nm and a digital integration time (D.I.T.) of 1 s. Each reported spectrum represents the average of three accumulations. Polymer samples were prepared in $CHCl_3$ under the same concentration conditions used for the CD measurements in the main text, and all CD samples were passed through a 0.22 μm syringe filter immediately before spectral acquisition to minimize dust and coarse particulates. The CD signal (mdeg) was acquired simultaneously with the PMT high-tension (HT) voltage and absorbance channels. A solvent baseline ($CHCl_3$), measured under identical conditions, was subtracted from each sample spectrum. To ensure data fidelity, spectral interpretation was limited to the detector's linear response region; following manufacturer guidance, data points exhibiting an HT voltage $\geqslant$ 700 V were excluded from the analysis (Supplementary Materials)[15].

2.4.6 Dynamic light scattering (DLS)

Hydrodynamic size distributions were analyzed using a Nanotrac Model NPA250 system (Microtrac Inc.) with $CHCl_3$ as the solvent at c = 0.2 mg mL^{-1}. Prior to analysis, all solutions were centrifuged at 3,600 rpm for 5 min to reduce interference from dust particles and large extrinsic artifacts. Measurements were conducted in triplicate to ensure statistical robustness; for each independent aliquot, two consecutive 60-second scans were performed. Data acquisition and processing were carried out using Microtrac FLEX software (version 10.3.14). Final size distributions are reported as the average of the three independent trials and plotted as intensity-weighted percentages versus hydrodynamic diameter.

2.4.7 Scanning electron microscopy (SEM)

Surface morphologies were imaged on a ZEISS Crossbeam 540 instrument (accelerating voltage: 5 kV; secondary electron detector). Samples were prepared by vacuum-drying polymer powders at 50 °C overnight, mounting them on adhesive carbon stubs, and sputter-coating with a thin gold layer to mitigate charging effects[13,14].

2.4.8 High-performance liquid chromatography

Enantiomeric excess was assessed via chiral HPLC on a Thermo Scientific UltiMate 3000 system (normal-phase). Samples (c = 1.0 mg mL^{-1}, 10 μL injection) were resolved on immobilized polysaccharide columns (DAICEL CHIRALPAK IA, IB, IC, or ID) using n-hexane/2-propanol (iPrOH) eluents.

2.4.9 High-resolution mass spectrometry (HRMS)

Mass spectra were acquired on a Thermo Scientific Orbitrap Fusion Lumos Tribrid spectrometer with an electrospray ionization (ESI) source. Samples were introduced by direct infusion in acetonitrile (CH_3CN) (c = 1 mg mL^{-1}), with data collected at a resolving power of

120,000 (FWHM at m/z 200).

2.4.10 Tyndall-effect test

Tyndall-effect observations were performed for polymer samples in $CHCl_3$ under the same concentration conditions used for the CD measurements. Prior to testing, all samples were filtered through a 0.22 μm syringe filter. Pure $CHCl_3$ was used as the blank control. The sample and blank were irradiated with the same laser source under identical conditions, and the resulting light paths were recorded for qualitative comparison.

3. Results and Discussion

3.1 Axial chirality as a design handle: monomer set and polymer construction

To examine how structural variations around the chiral axis influence subsequent polymer formation and aggregation behavior, we prepared a deliberately comparable set of enantiopure 8,8'-dibrominated binaphthyl monomers. The syntheses followed established procedures with modest adjustments (Figure 1)[11,12]. Throughout the series, the 7,7'-dimethoxy core was retained in order to minimize changes in the underlying binaphthyl framework and to focus structural variation at the 2,2'-positions.

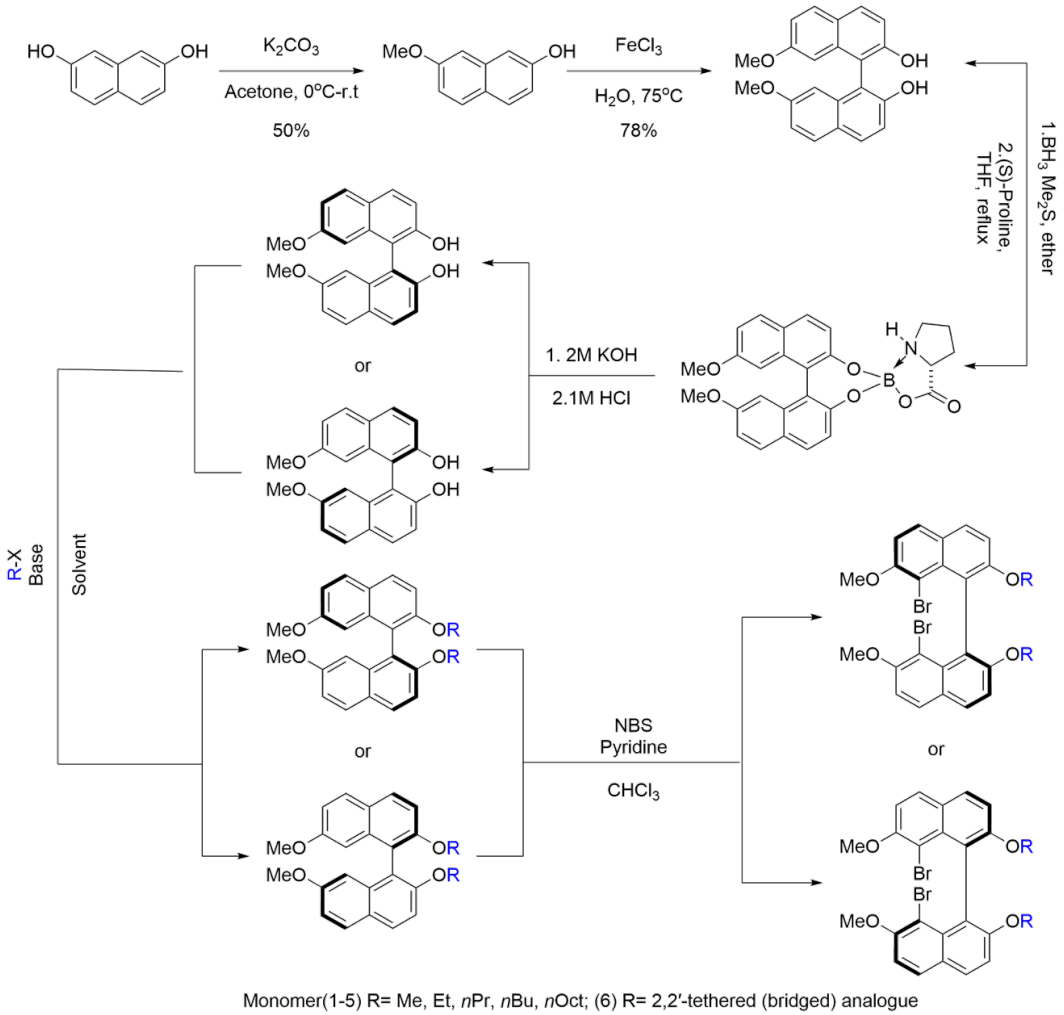

Figure 1. Preparation of axially chiral monomers.

The primary subset of the library consists of a homologous alkoxy series in which the principal variable is side-chain length: [**1***S*/*R* (MeO), **2***S*/*R* (EtO), **3***S*/*R* (*n*PrO), **4***S* (*n*BuO), and **5***S* (*n*OctO)]. This set was designed to provide a gradual increase in peripheral steric demand and hydrophobicity without altering the axial linkage itself (Figure 2).

We also prepared a more conformationally restricted counterpart, **6***S* (Figure 2), in which the 2,2'-positions are connected through a dioxine tether. This bridge limits conformational flexibility around the chiral axis and imposes a more preorganized local geometry relative to the alkoxy-substituted analogues[5,6]. In this sense, **6** represents not merely a sterically modified member of the same series, but a distinct structural motif with a different mode of conformational control.

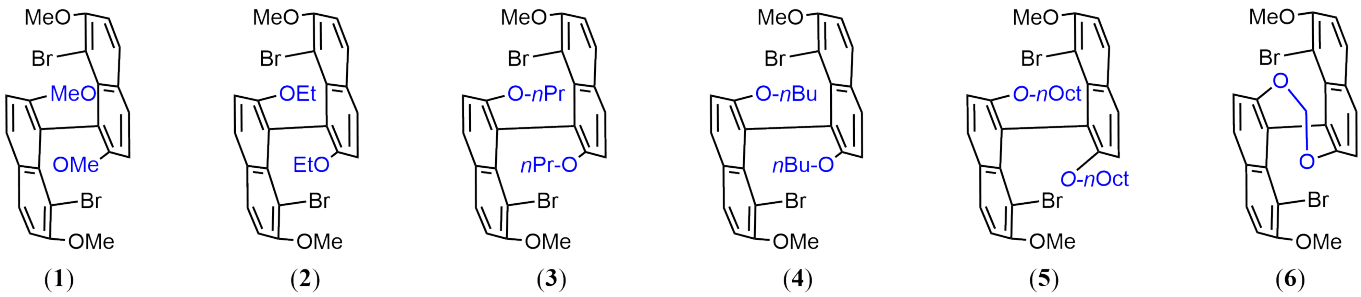

Figure 2. Axially chiral monomers **1–6**.

Structures and enantiopurities for all monomers were verified by NMR and chiral HPLC (Supplementary Materials). Together, monomers **1**–**5** provide a flexible series for evaluating the effects of progressively varied peripheral crowding and hydrophobicity, whereas **6** provides a tether-enforced reference for examining the consequences of more rigid conformational restriction. This monomer set therefore offers a useful basis for assessing how relatively subtle peripheral changes, as compared with more pronounced geometric constraint, influence the expression of axial stereochemistry in the resulting multilayer polymers.

Polymerization was carried out via Sonogashira cross-coupling at the 8,8'-positions, using 1,8-diethynylnaphthalene as the diyne bridge to incorporate the binaphthyl axial twist into the conjugated backbone while maintaining the targeted nonplanar multilayer framework (Figure 3). Under these conditions, a library of nine polymers was obtained, comprising the enantiomeric pairs **1A***R*/*S*, **2A***R*/*S*, and **3A***R*/*S* together with the extended analogues **4AS**, **5AS**, and **6AS**. After purification by repeated precipitation and washing to remove oligomeric fractions, the target polymers were isolated in yields ranging from 14 to (Table 1).

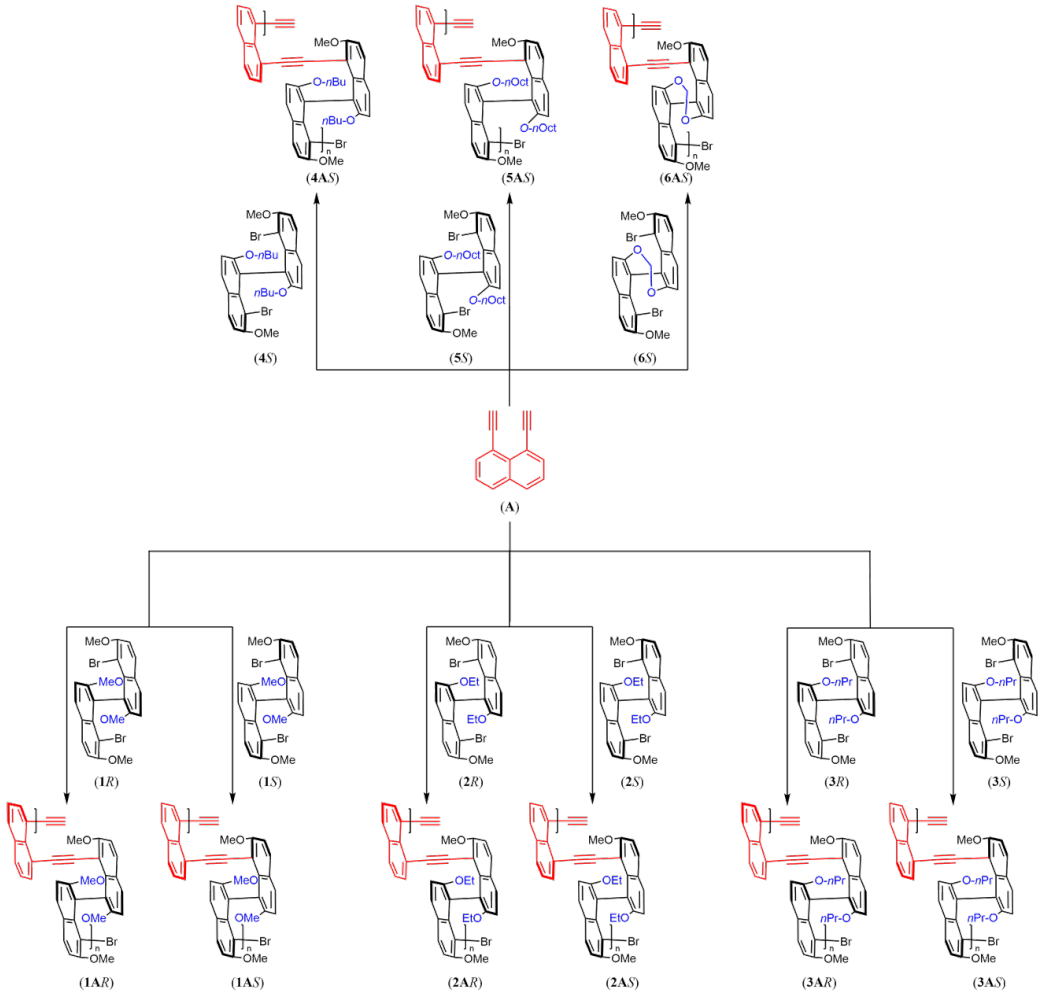

Figure 3. Synthesis of the axially chiral multilayer polymers **1A–6A**.

Table 1. Synthetic results and molecular weights of the polymers.

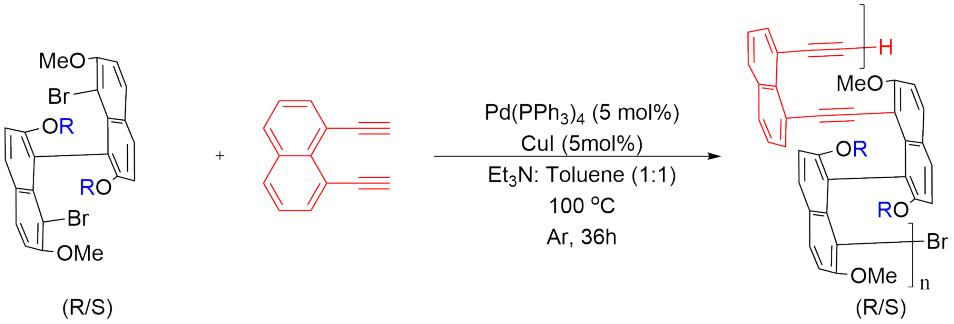

Entry	Polymer	Yield[a] (%)	M_n[b]	M_w[b]	PDI[c]
1	**1A***R*	19	5,606	7,730	1.379
2	**1A***S*	35	5,841	7,921	1.356
3	**2A***R*	25	5,192	7,378	1.421
4	**2A***S*	25	6,255	9,053	1.447
5	**3A***R*	22	5,511	7,240	1.314
6	**3A***S*	21	5,457	7,567	1.387
7	**4A***S*	18	5,986	9,462	1.581
8	**5A***S*	14	4,135	5,939	1.436
9	**6A***S*	27	4,912	6,667	1.357

[a]: Isolated yield based on substrates **1–6** and **A**; [b]: Determined by GPC using polystyrene standards; [c]: PDI = M_w/M_n; GPC: gel permeation chromatography; PDI: polydispersity index.

3.2 Molecular weight analysis (GPC)

As summarized in Table 1, GPC analysis indicated moderate molecular weights across the polymer library (M_n = 4,135–6,255 g mol^{-1}; M_w = 5,939–9,462 g mol^{-1}) with relatively narrow dispersities (PDI = 1.31–1.58). Overall, these data are consistent with successful polymer formation across the series under the applied conditions. Representative chromatograms, instrumental parameters, and calibration details are provided in the Supplementary Materials.

3.3 Chiroptical signatures and stereochemical fidelity (CD)

An important question in this work is whether the axial chirality encoded in the monomers is retained after polymerization. CD spectroscopy provides chiroptical evidence that stereochemical information is preserved in the resulting polymer systems under the tested CHCl3 measurement conditions. To assess data quality and minimize instrumental artifacts, CD spectra were recorded together with the HT voltage (PMT high tension) and absorbance channels. For the samples shown in the main text (**1A**–**3A**), the HT traces remain well below the manufacturer-recommended cutoff throughout the analyzed window, supporting that the reported CD features are not dominated by low-light/PMT-limit noise (Figures S92-S94 for combined CD/HT/Abs panels in Supplementary Materials)[15,16]. Taken together, the DLS, UV baseline, and Tyndall-effect results indicate that the $CHCl_3$ samples are best described as aggregation-sensitive polymer dispersions under the measurement conditions. The CD spectra therefore report the chiroptical behavior of these polymer systems under the tested conditions, while still supporting retention of stereochemical information after polymerization.

For the enantiomeric pairs **1A**–**3A**, the CD spectra display Cotton effects of opposite sign with broadly complementary, but not perfectly mirror-symmetrical, line shapes (Figure 4). This behavior is consistent with chiroptical responses arising from the corresponding *R*- and *S*-configured polymer systems, while also indicating that the detailed spectral shapes remain sensitive to polymer-sample differences and aggregation state under the tested conditions[17-19]. The most intense feature appears in the 250–290 nm region. At longer wavelengths (300–400 nm), a weaker contribution of opposite sign becomes discernible, most clearly for **1A** and **2A**, giving a partially resolved bisignate profile. Such bisignate signatures are consistent with exciton-coupled interactions between proximate aromatic chromophores and therefore support the presence of inter-unit electronic coupling within the multilayer backbone[20].

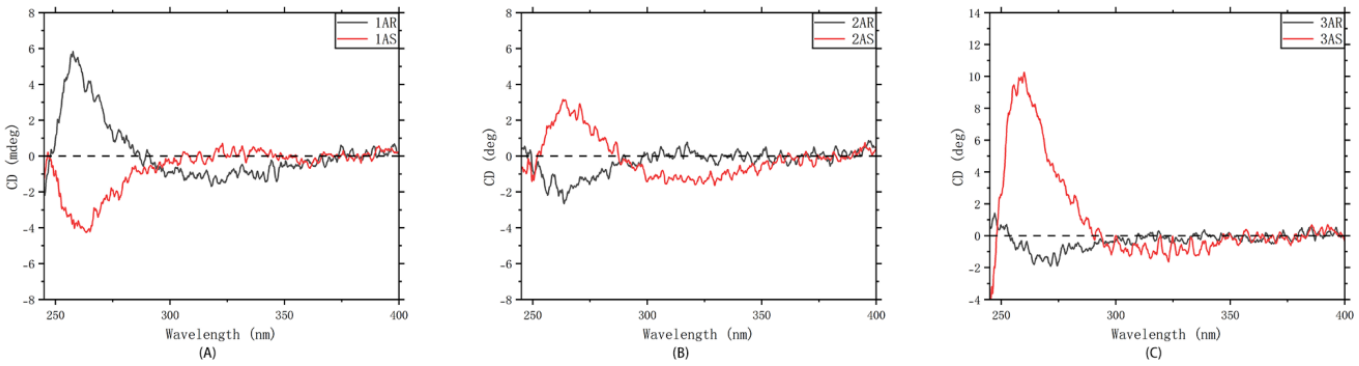

Figure 4. CD spectra of polymers **1A–3A** (enantiomeric pairs). (A) Polymer **1A** (**1A***R*/**1A***S*); (B) Polymer **2A** (**2A***R*/**2AS**); (C) Polymer **3A** (**3A***R*/**3A***S*). CD: circular dichroism.

To probe how chain connectivity and conformational restriction influence chiroptical expression, CD spectra were also acquired for the longer-chain analogues (**4AS**, **5AS**) and the tethered analogue (**6AS**) (Supplementary Materials). These polymers likewise exhibit measurable Cotton effects in the aromatic region, supporting retention of chiral information after polymerization. Notably, the tethered polymer **6AS** shows a pronounced Cotton effect, consistent with stronger chiroptical expression in a more conformationally constrained scaffold. Likewise, the octyl-substituted polymer **5AS** exhibits a clearer bisignate profile, suggesting that the more extended alkyl substituent can alter the local packing environment and the associated chiroptical response under the tested conditions.

3.4 Backbone spectroscopic signatures (UV–vis absorption)

The UV–vis absorption profiles of polymers **1A**–**6A** in $CHCl_3$ are shown in Figure 5. The spectra are dominated by high-intensity absorptions centered at ≈ 245 nm, which are assigned to localized aromatic $\pi \rightarrow \pi^*$ transitions of the binaphthyl chromophores[21]. Accompanying this primary band is a broader, lower-intensity absorption manifold extending from 300 to 400 nm. In conjugated systems, this region is often sensitive to backbone torsion and inter-unit electronic coupling, both of which can influence the effective conjugation length and the associated transition energies[22].

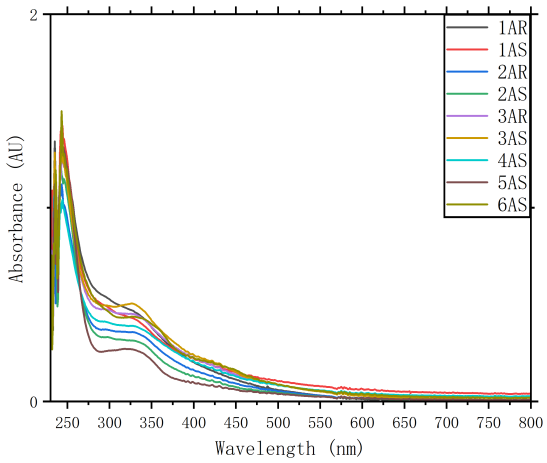

Figure 5. UV–vis absorption spectra of polymers **1A–6A** in $CHCl_3$ (c = 0.05 mg mL^{-1}).

Across the linear alkoxy series (**1A**–**5A**), the polymers display broadly comparable spectral envelopes, suggesting that variation of the side-chain length from methoxy to octyloxy only modestly perturbs the ground-state electronic transitions of the binaphthyl-centered framework. The tethered analogue **6AS**, however, exhibits a somewhat broadened absorption profile in the 300–400 nm region. This behavior is consistent with the conformational restriction imposed by the rigid dioxine bridge, which can narrow the accessible dihedral angle distribution and alter inter-unit electronic coupling relative to the open-chain analogues[6].

Extension of the spectral window to 800 nm reveals two additional features in the visible region. First, rather than showing a sharp cutoff, the spectra display a gradual trailing edge from 400 to ≈ 600 nm. This baseline elevation is consistent with wavelength-dependent light scattering from dispersed aggregates under the measurement conditions, in agreement with the DLS results and further supported by the Tyndall-effect observations shown in Figure S95-S101[23]. Second, beyond 600 nm the absorbance approaches the baseline for all samples, indicating that no pronounced low-energy electronic transitions are resolved in this region within the sensitivity of the present measurements.

3.5 Aggregation behavior and morphology (PL, DLS, and SEM)

To probe how backbone rigidity and side-chain sterics regulate aggregation and emission behavior, we recorded PL spectra for the full polymer library (**1**–**6**) in THF/H2O mixtures with water fractions (f_w) ranging from 10% to 90%. In an achiral medium, enantiomeric pairs are expected to exhibit identical scalar photophysical properties, whereas chirality is manifested in differential observables such as CD or circularly polarized luminescence (CPL)[24]. Accordingly, the spectroscopic series for the -configured polymers (**1A*S***–**6A*S***) are shown in Figure 6 to highlight structure-dependent trends. The corresponding spectra for the *R*-enantiomers (**1A*R***–**3A*R***) show essentially identical composition-dependent PL behavior and are therefore provided in the Supplementary Materials.

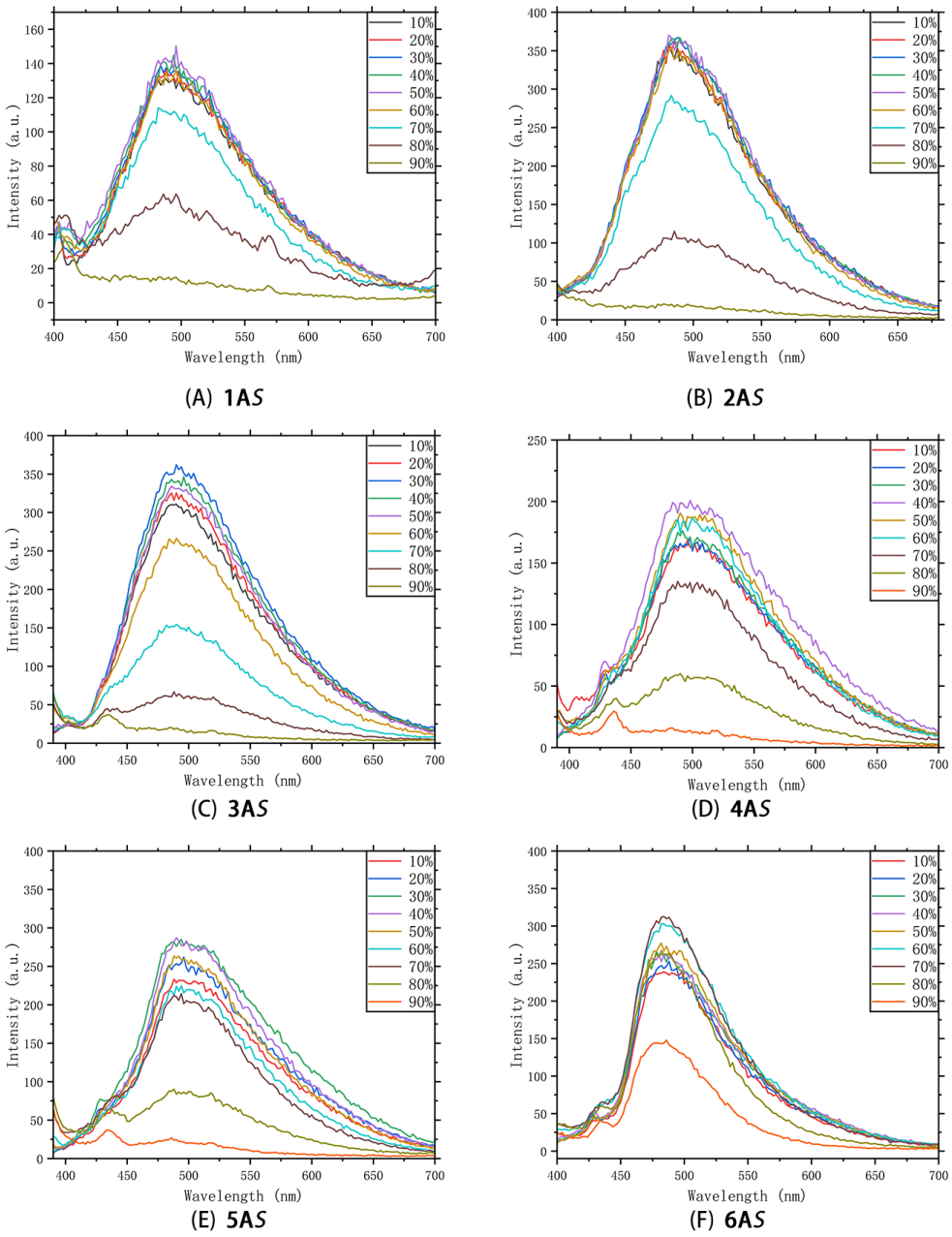

Figure 6. Solvent-dependent PL spectra of the -configured polymer series (**1A*S*–6A*S***) in THF/H_2O mixtures with varying water fractions (f_w). All polymers exhibit an initial AIE-like enhancement followed by quenching at high water fractions. Experimental conditions: c = 0.05 mg mL^{-1}; λ_{ex} = 380 nm; slit widths (Ex/Em) = 5/5 nm; PMT voltage = 800 V. PL: photoluminescence.

Across the series, the emission response is distinctly non-monotonic as a function of f_w. In pure THF, the polymers exhibit relatively weak emission, consistent with active intramolecular motions that facilitate nonradiative decay. Upon increasing f_w the emission intensity rises markedly in the low-to-intermediate regime, showing AIE-like enhancement that is consistent with aggregate-induced restriction of intramolecular motions[8,9].

The water fraction at which emission turns over from enhancement to quenching depends strongly on polymer architecture. For the linear alkoxy-substituted polymers (**1AS**–**5AS**, Figure 6A,B,C,D,E), the emission typically reaches a maximum at $f_W \approx 40$–50% and then decreases at higher water content. This behavior indicates that increasing water fraction progressively changes the aggregate state, and that more strongly associated species formed at higher fw promote additional nonradiative deactivation. In this sense, the emission decrease at higher water fractions is consistent with ACQ-like behavior in more densely aggregated states[25,26]. Extending the alkyl side chain in **5AS** moderates, but does not eliminate, the quenching tendency, suggesting that backbone–backbone interactions remain an important determinant of packing in the aggregated state.

In contrast, the tethered polymer **6AS** (Figure 6F) maintains emission enhancement up to higher f_W (ca.) before quenching becomes dominant. This delayed turnover is consistent with the conformational restriction imposed by the locked binaphthyl scaffold, which may disfavor overly intimate packing and thereby sustain an emissive aggregated state over a broader composition range. At very high water fractions (f_W > 80%), all systems ultimately exhibit pronounced quenching, consistent with the formation of more strongly associated aggregated states and enhanced interchain interactions in water-rich mixtures[25].

DLS indicates the presence of large dispersed species for these polymers in $CHCl_3$ under the measurement conditions. As shown in Figure 7, the *intensity-weighted* size distributions for all entries (**1A**–**6A**) are dominated by scattering species with apparent hydrodynamic diameters (D_h) in the 1,000-2,000 nm range. The error bars derived from triplicate measurements support the reproducibility of this overall trend.

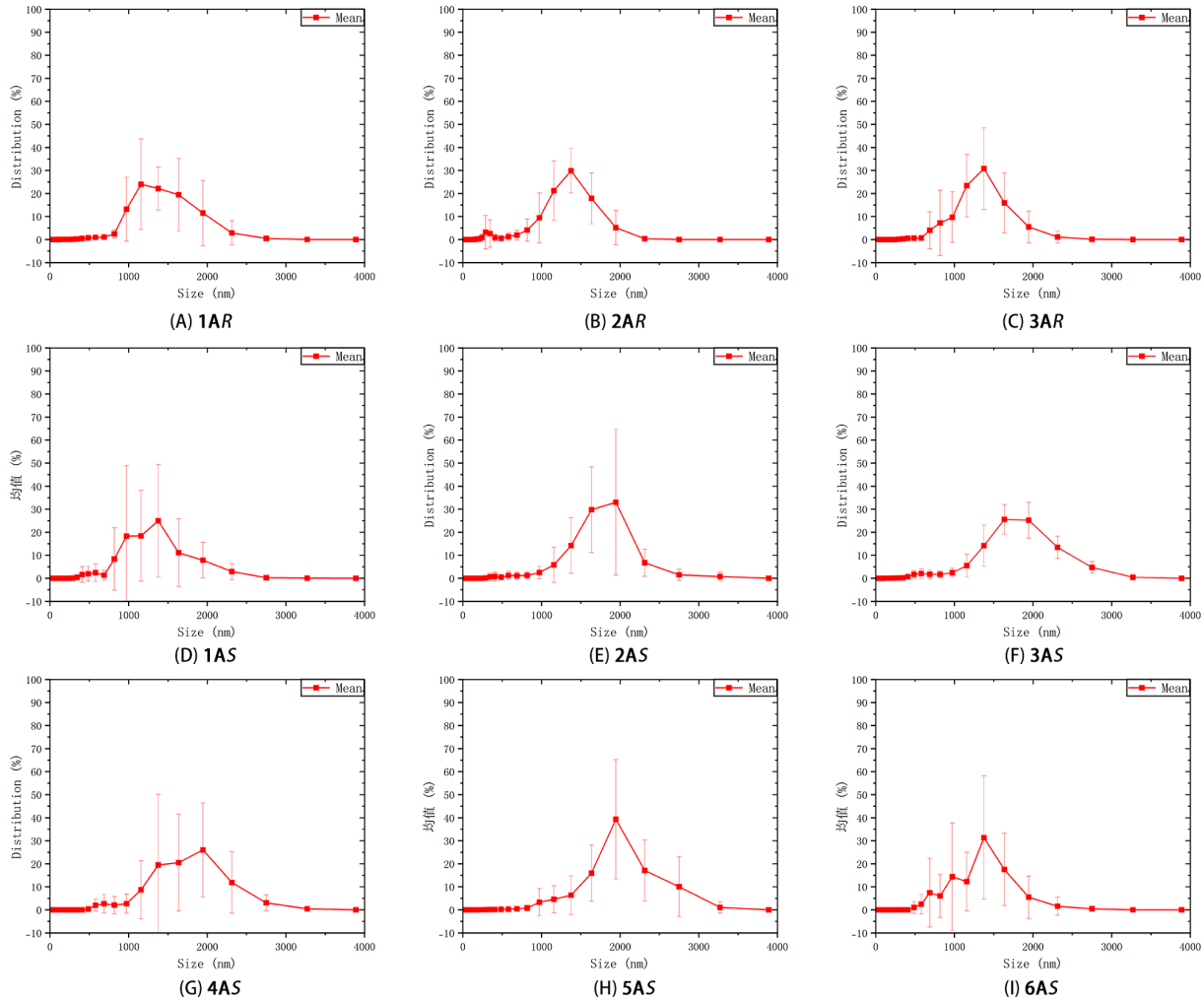

Figure 7. DLS size distributions of polymers in $CHCl_3$ (c = 0.2 mg mL^{-1} *intensity-weighted*). DLS: dynamic light scattering.

Because DLS reports an intensity-weighted distribution, larger scatterers can disproportionately dominate the signal; under the Rayleigh approximation, the scattering intensity scales approximately with the sixth power of particle size, such that even a minor population of micron-scale aggregates can overwhelm contributions from smaller, more molecularly dispersed species[23,27]. We therefore interpret the micron-scale mode as evidence for a significant population of large, solvent-associated dispersed aggregates under the tested conditions, while noting that DLS alone does not resolve aggregate morphology[27,28].

These large scatterers are also consistent with the wavelength-dependent baseline elevation observed in the UV–vis spectra and may contribute to attenuation or distortion of chiroptical signals in more turbid samples. Accordingly, we treat DLS, UV–vis, and CD as complementary indicators of aggregation-sensitive behavior rather than as a strict one-to-one correspondence between techniques[29-31].

SEM provides dried-state morphological context for polymers **1A**–**6A** (Figure 8A,B,C,D,E,F,G,H,I). Across the series, the materials appear as hierarchical agglomerated structures, in which submicrometer particulates further cluster into larger, irregular micrometer-scale domains with granular surface textures.

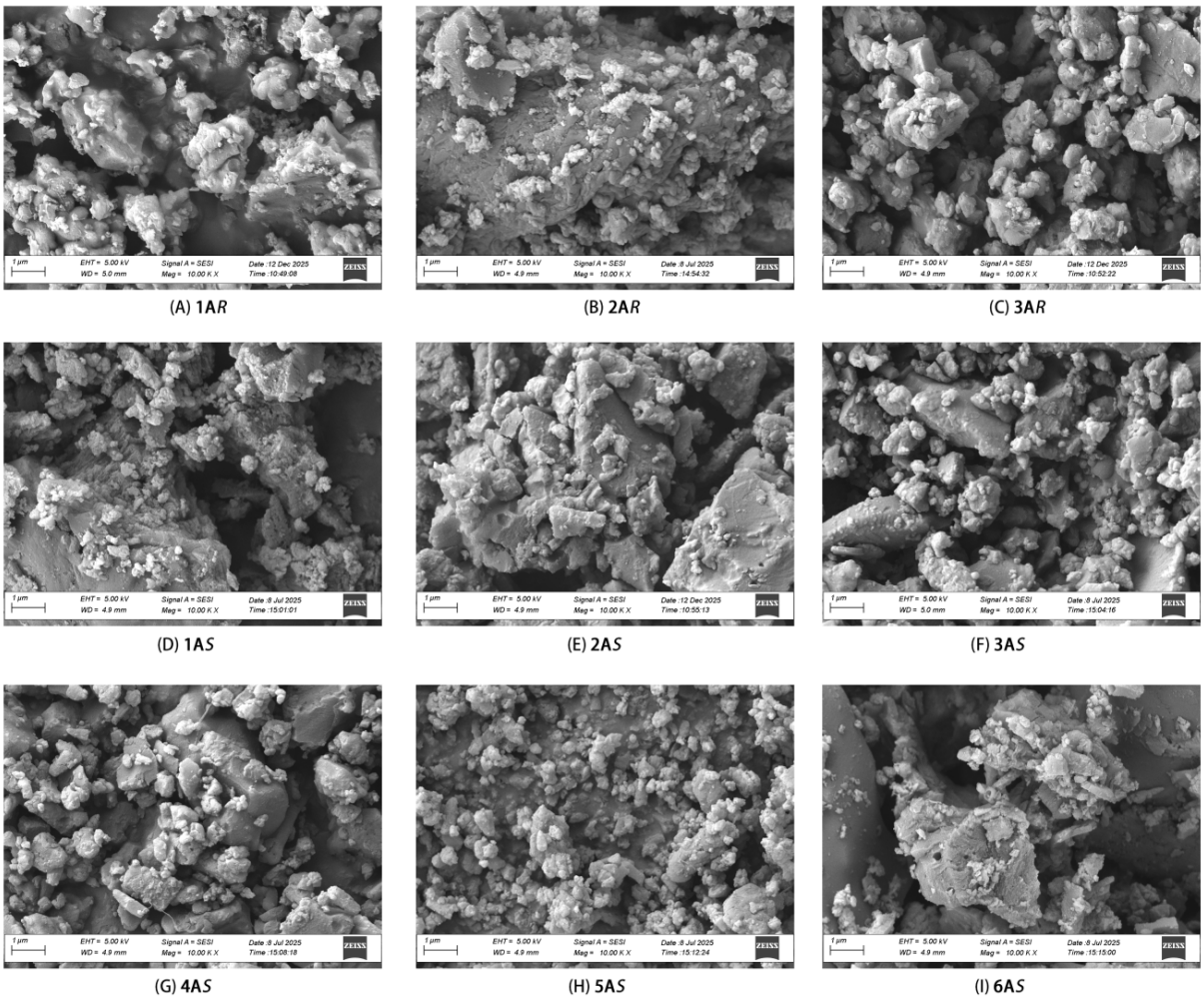

Figure 8. Representative SEM images of polymers **1A–6A**. SEM: scanning electron microscopy.

Because SEM imaging was performed under vacuum on dried and metal-coated specimens, solvent removal and sample preparation may induce shrinkage, rearrangement, or secondary aggregation in these materials. The micrographs are therefore interpreted as qualitative dried-state morphological information rather than as a direct one-to-one representation of native solution-state assemblies[13,14].

Nevertheless, the recurrence of these hierarchical agglomerated features across multiple fields of view and magnifications (Supplementary Materials) indicates a pronounced tendency toward aggregate formation under the preparation conditions. This observation is qualitatively consistent with the presence of large dispersed species detected by DLS, and we therefore treat SEM and DLS as complementary indicators of aggregation-related behavior under their respective measurement conditions.

4. Conclusion

This study establishes a robust synthetic platform for accessing the first enantiopure, axially chiral multilayer 3D folding polymers featuring structurally compacted triple-column/multiple-layer frameworks. Building on earlier multicolumn/multilayer 3D polymer frameworks and their chiral variants, we translated the monomer-defined axial twist of 8,8'-functionalized binaphthyl building blocks into extended conjugated backbones via Sonogashira polycondensation.

The structural dichotomy of the monomer library, contrasting the flexible alkoxy series (**1**–**5**) with the conformationally constrained tethered analogue (**6**), provides useful design insight into how steric environment and backbone rigidity influence the expression of axial chirality at the macromolecular level. In particular, the pronounced chiroptical response of the tethered polymer **6AS** is consistent with the view that conformational restriction can enhance chiroptical expression and may improve the robustness of stereochemical readout during polymer formation.

Beyond molecular design, multiscale characterization (UV/CD, PL, DLS, SEM) reveals a pronounced tendency toward aggregation-related behavior under the respective measurement conditions. DLS in $CHCl_3$ and SEM of dried deposits indicate hierarchical organization spanning submicrometer particulates to micrometer-scale agglomerated domains, while PL in THF/H_2O mixtures shows AIE-like enhancement at intermediate water fractions followed by quenching in more water-rich mixtures. These results support the view that aggregation is a key mediator of the observed optoelectronic behavior, linking solvent environment to packing-dependent nonradiative pathways. Importantly, the opposite-signed CD spectra observed for the enantiomeric pairs (**1A**–**3A**) support retention of chiral information under the tested CHCl3 conditions, while the evolution of CD line shapes suggests that aggregation-sensitive organization also contributes to the overall chiroptical response.

Collectively, these results advance axially chiral multilayer backbones toward a more rationally designable class of functional polymeric materials. Future studies will focus on translating aggregation-dependent chiroptical behavior into practical readouts and devices, including CPL and enantioselective sensing, where control over hierarchical assembly and local chromophore arrangement may prove advantageous[32].

Supplementary materials

The supplementary material for this article is available at: Supplementary materials.

Declarations

Acknowledgments

ChatGPT (OpenAI, GPT-5 series model) was used solely for language editing and polishing of the manuscript, including improving grammar, readability, and sentence flow. No AI tool was used to generate, analyze, or interpret experimental data, draw scientific conclusions, or create original research figures. All authors reviewed and edited the manuscript and take full responsibility for the integrity, accuracy, and originality of the final content.

Authors contribution

Liu H: Investigation, formal analysis, writing-original draft.
Yuan Q: Investigation.
Lina DC, Cozzolino AF: Formal analysis.
Akinpelu ZM, Phan M: Investigation.
Liang H, Pappas D: Formal analysis.
Li G: Supervision, writing-review & editing
All authors read and approved the final manuscript.

Conflicts of interest

The authors declare no conflicts of interest.

Ethical approval

Not applicable.

Consent to participate

Not applicable.

Consent for publication

Not applicable.

Availability of data and materials

The data that support the findings of this study are available from the corresponding author upon reasonable request.

Funding

The authors acknowledge financial support from the Robert A. Welch Foundation (Grant No. D-1361-20210327) and the National Natural Science Foundation of China (Grant Nos. 22071102 and 91956110).

Copyright

© The Author(s) 2026.

References

1. Takata T, Furusho Y, Murakawa KI, Endo T, Matsuoka H, Hirasa T, et al. Optically active poly(aryl carbonates) consisting of axially chiral units. chiral binaphthyl group induced helical polymer. J Am Chem Soc. 1998;120(18):4530-4531. [DOI]
2. Ritter N, Senkovska I, Kaskel S, Weber J. Towards chiral microporous soluble polymers: Binaphthalene-based polyimides. Macromol Rapid Commun. 2011;32(5):438-443. [DOI][PubMed]
3. Tang Y, Jin S, Zhang S, Wu GZ, Wang JY, Xu T, et al. Multilayer 3D chiral folding polymers and their asymmetric catalytic assembly. Research. 2022;2022:2022/9847949. [DOI]
4. Zhang S, Yuan Q, Li G. New multiple-layered 3D polymers showing aggregation-induced emission and polarization. RSC Adv. 2024;14(19):13342-13350. [DOI][PubMed][PMC]
5. Pu L. Regioselective substitution of BINOL. Chem Rev. 2024;124(10):6643-6689. [DOI][PubMed][PMC]
6. Ikai T, Mishima N, Matsumoto T, Miyoshi S, Oki K, Yashima E. 2, 2'-tethered binaphthyl-embedded one-handed helical ladder polymers: Impact of the tether length on helical geometry and chiroptical property. Angew Chem Int Ed. 2024;63(10):e202318712. [DOI][PubMed]
7. Wang Y, Li Y, Liu S, Li F, Zhu C, Li S, et al. Regulating circularly polarized luminescence signals of chiral binaphthyl-based conjugated polymers by tuning dihedral angles of binaphthyl moieties. Macromolecules. 2016;49(15):5444-5451. [DOI]
8. Hong Y, Lam JWY, Tang BZ. Aggregation-induced emission. Chem Soc Rev. 2011;40(11):5361. [DOI]
9. Mei J, Leung NL, Kwok RT, Lam JW, Tang BZ. Aggregation-induced emission: Together we shine, united we soar! Chem Rev. 2015;115(21):11718-11940. [DOI][PubMed]
10. Tsuji H, Nakahata M, Hishida M, Seto H, Motokawa R, Inoue T, et al. Water fraction dependence of the aggregation behavior of hydrophobic fluorescent solutes in water-tetrahydrofuran. J Phys Chem Lett. 2023;14(49):11235-11241. [DOI][PubMed][PMC]
11. Gong B, Chen W, Hu B. A new and efficient method for the resolution of 2, 2'-dihydroxy-1, 1'-binaphthyl. J Org Chem. 1991;56(1):423-425. [DOI]
12. Tang Y, Yuan Q, Zhang S, Wang JY, Surowiec K, Li G. Enantioselective synthesis of [1, 1'-binaphthalene]-8, 8'-diyl bis(diphenylphosphane) and its derivatives. RSC Adv. 2024;14(4):2792-2795. [DOI][PubMed][PMC]
13. Goldstein JI, Newbury DE, Michael JR. Scanning electron microscopy and X-ray microanalysis. New York: Springer New York; 2017. [DOI]
14. Heu R, Shahbazmohamadi S, Yorston J, Capeder P. Target material selection for sputter coating of SEM samples. Micros Today. 2019;27(4):32-36. [DOI]
15. JASCO. Circular dichroism tips & tricks (ht voltage guidance) [Internet]. 2018. Available from: https://jascoinc.com/wp-content/uploads/2018/03/CD-Tips-Tricks-Printable-3.18.pdf
16. Ugras TJ, Yao Y, Robinson RD. Can we still measure circular dichroism with circular dichroism spectrometers: The dangers of anisotropic artifacts. Chirality. 2023;35(11):846-855. [DOI][PubMed]
17. Berova N, Nakanishi K, and Woody RW. Circular dichroism: Principles and applications. 2nd ed. Hoboken: John Wiley & Sons; 2000.
18. Van Oosten A, Verduyckt C, De Winter J, Gerbaux P, Koeckelberghs G. Influence of the dispersity and molar mass distribution of conjugated polymers on the aggregation type and subsequent chiral expression. Soft Matter. 2023;19(21):3794-3802. [DOI]
19. Fujiki M, Okazaki S, Rahim NAA, Yamada T, Nomura K. Synchronization in non-mirror-symmetrical chirogenesis: Non-helical π–conjugated polymers with helical polysilane copolymers in co-colloids. Symmetry. 2021;13(4):594. [DOI]
20. Pescitelli G. ECD exciton chirality method today: A modern tool for determining absolute configurations. Chirality. 2022;34(2):333-363. [DOI]
21. Taniguchi M, Lindsey JS. Database of absorption and fluorescence spectra of > 300 common compounds for use in PhotochemCAD. Photochem Photobiol. 2018;94(2):290-327. [DOI][PubMed]
22. Kanimozhi C, Naik M, Yaacobi-Gross N, Burnett EK, Briseno AL, Anthopoulos TD, et al. Controlling conformations of diketopyrrolopyrrole-based conjugated polymers: Role of torsional angle. J Phys Chem C. 2014;118(22):11536-11544. [DOI]
23. Stetefeld J, McKenna SA, Patel TR. Dynamic light scattering: A practical guide and applications in biomedical sciences. Biophys Rev. 2016;8(4):409-427. [DOI][PubMed][PMC]
24. Brooks WH, Guida WC, Daniel KG. The significance of chirality in drug design and development. Curr Top Med Chem. 2011;11(7):760-770. [DOI][PubMed][PMC]
25. Huang Y, Xing J, Gong Q, Chen LC, Liu G, Yao C, et al. Reducing aggregation caused quenching effect through co-assembly of PAH chromophores and molecular barriers. Nat Commun. 2019;10(1):169. [DOI][PubMed][PMC]
26. Zhang K, Liu J, Zhang Y, Fan J, Wang CK, Lin L. Theoretical study of the mechanism of aggregation-caused quenching in near-infrared thermally activated delayed fluorescence molecules: Hydrogen-bond effect. J Phys Chem C. 2019;123(40):24705-24713. [DOI]
27. Filippov SK, Khusnutdinov R, Murmiliuk A, Inam W, Zakharova LY, Zhang H, et al. Dynamic light scattering and transmission electron

microscopy in drug delivery: A roadmap for correct characterization of nanoparticles and interpretation of results. Mater Horiz. 2023;10(12):5354-5370. [DOI][PubMed]
28. Jia Z, Li J, Gao L, Yang D, Kanaev A. Dynamic light scattering: A powerful tool for in situ nanoparticle sizing. Colloids Interfaces. 2023;7(1):15. [DOI]
29. Basalla AJ, Kendrick BS. Correcting ultraviolet-visible spectra for baseline artifacts. J Pharm Sci. 2023;112(12):3240-3247. [DOI][PubMed]
30. Chakraborty H, Lentz BR. A simple method for correction of circular dichroism spectra obtained from membrane-containing samples. Biochemistry. 2012;51(5):1005-1008. [DOI][PubMed][PMC]
31. Miles AJ, Janes RW, Wallace BA. Tools and methods for circular dichroism spectroscopy of proteins: A tutorial review. Chem Soc Rev. 2021;50(15):8400-8413. [DOI][PubMed][PMC]
32. Li SY, Xu L, Gao RT, Chen Z, Liu N, Wu ZQ. Advances in circularly polarized luminescence materials based on helical polymers. J Mater Chem C. 2023;11(4):1242-1250. [DOI]

Publisher's Note

Science Exploration remains a neutral stance on jurisdictional claims in published maps and institutional affiliations. The views expressed in this article are solely those of the author(s) and do not reflect the opinions of the Editors or the publisher.